ACS APPLIED POLYMER MATERIALS

pubs.acs.org/acsapm Article

On the Temperature Dependence of the Piezoelectric Response of Prepoled Poly(vinylidene fluoride) Films

Jeffrey D. Sherman,*[,§] Jeffrey Elloian,[§] Jakub Jadwiszczak, and Kenneth L. Shepard

Cite This: https://dx.doi.org/10.1021/acsapm.0c00902 Read Online

ACCESS | Metrics & More | Article Recommendations | Supporting Information

ABSTRACT: There is growing interest in integrating piezoelectric materials with complementary metal-oxide-semiconductor (CMOS) technology to enable expanded applications. A promising material for ultrasound transducer applications is poly(vinylidene fluoride) (PVDF), a piezoelectric polymer. One of the challenges with PVDF is that its piezoelectric properties can deteriorate when exposed to temperatures in excess of 70 °C for extended periods of time during fabrication. Here, we report on the effects of both shortening annealing times and providing this heating nonuniformly, as is characteristic of some processing conditions, on the piezoelectric coefficient (d_{33}) of PVDF films for various thicknesses. In this case, no degradation in the d_{33} was observed at temperatures below 100 °C for anneal times of under 1 min when this heating is applied through one side of the film, making PVDF compatible with many bonding and photolithographic processing steps required for CMOS integration. More surprisingly, for one-sided heating to temperatures between 90 and 110 °C, we observed a transient enhancement of the d_{33} by nearly 40% that lasted for several hours after these anneals. We attribute this effect to induced strain in these films.

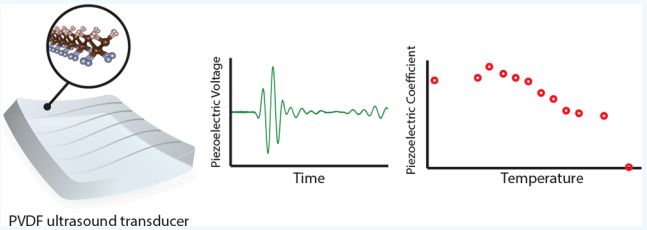

KEYWORDS: *poly(vinylidene fluoride), piezoelectric, temperature, characterization, ultrasound, transducer*

INTRODUCTION

In the last decade, interest in the miniaturization of ultrasonic technology for integrated circuit applications has surged.[1−3] From on-chip resonators[4] and multimodal sensors,[5,6] to energy harvesters[7−10] and biomedical applications,[11] the need for biocompatible piezoelectric transducers integrated with CMOS-based electronics has grown. While capacitive micromachined ultrasound transducers (CMUTs) offer a possible CMOS-compatible solution, their high bias voltages,[12] limitations on carrier frequency (<50 MHz), and involved fabrication processes present challenges. Bulk piezoelectric transducer elements, which require no biasing and which can take the form of ceramics or polymers, do not have these limitations and have found applications in integrated electronics.[13,14] Ceramic materials, such as lead zirconate titanate, tend to have a high acoustic impedance, which necessitates a matching layer for effective performance. Further, the intrinsically high quality (Q) factor of these materials limits their bandwidth for many applications.[13] On the other hand, piezoelectric polymers such as PVDF have acoustic impedances close to that of human tissue, eliminating the need for a matching layer.[15] In addition, unlike ceramics, PVDF has a relatively low Q, allowing for high-bandwidth ultrasonic elements.

The piezo-active phase of PVDF is the β phase, where electronegative fluorine atoms are in an all-*trans* configuration relative to the hydrogen atoms in the alkane-like polymer chain.[16,17] This configuration yields a significant electric dipole moment in the out-of-plane crystallographic b direction, perpendicular to the direction of the long polymer chains.[18] The β phase is usually obtained by mechanical pulling and/or heating of the piezo-inactive α phase,[19−24] and its piezoelectric coefficient (d_{33}) is a function of the film thickness and the exact ratio of phase content in the material. To activate meaningful piezoelectric functionality, the solid-state β-PVDF films are then poled at high electric fields (~5000 kV cm^{-1}).[25] With these poling approaches, bulk PVDF has been used to successfully generate pressure waves with center frequencies, f > 100 MHz,[26] while spin-casting and lithographic techniques have yielded elements with f > 300 MHz.[27]

These poling requirements make integration of PVDF transducers with CMOS difficult. The polymer can be spin-cast, but these techniques require poling after deposition, and the fields needed for the poling process have magnitudes well above the tolerance of standard CMOS circuits.[25,27] To circumvent this limitation, prepoled films can be bonded to a substrate. Reported bonding solutions include metal−metal

Received: August 19, 2020
Accepted: August 27, 2020
Published: August 27, 2020

bonding processes[28] and thin epoxy-based solutions,[29] but these methods fail when the contact area is on the order of micrometers. Bonding approaches are further complicated by thermal budgets. β-PVDF degrades when the material is exposed to temperatures above 70 °C for extended periods of time.[22] The apparent origin of this decay is the release of trapped surface charge due to the thermal destabilization of the semicrystalline polymer domains.[30,31] Photolithographic and bonding processes often require short baking steps carried out at temperatures >70 °C; thus, utilizing prepoled films in a manner that preserves their d_{33} after thermal processing is an important challenge to overcome to integrate PVDF into CMOS technology.

Here, we investigate the effects of short anneals representative of the baking steps required for bonding and lithography on the piezoelectric properties of PVDF for a range of polymer film thicknesses. We record changes in the d_{33} on a PVDF film caused by one-sided conductive heating (unidirectional heating). We observe that these short unidirectional anneals, which mimic lithographic process conditions, have almost no permanent effects on the piezoelectric properties of PVDF when the temperature is kept below ∼100 °C. We characterize the changes in the crystal structure and surface of the heated β-phase PVDF films and find that they correlate strongly with changes to d_{33}, further supporting the theory that thermally induced random depolarization is responsible for the loss of piezoelectricity in PVDF. We compare these changes with changes caused by conductive heating from both sides (or bidirectional heating). We find evidence that increased sample strain caused by unidirectional heating correlates with a reduced depolarization, yielding a higher long-term d_{33} value. Finally, we observe an anomalous transient boost in the d_{33} of PVDF immediately following the unidirectional annealing, lasting up to 72 hours, which we link to the mechanical deformation caused by the induced strain.

EXPERIMENTAL SECTION

Materials and Heating. β-PVDF samples (∼1 cm^2 in area) were cut from single sheets of commercially available unmetallized films of various thicknesses: 28 μm (Precision Acoustics), 110 μm (Kureha), and 200 μm (Kureha). Metallized PVDF provides structural support that inhibits the mechanical changes that we believe dominate the responses in this experiment. The heating stage of a submicrometer bonder (Finetech FINEPLACER lambda) was used to accurately control the sample temperature, ramping up to a target temperature at a rate of 5 °C s^{-1} and holding it constant for 60 s, after which the sample was removed and cooled rapidly to ambient room temperature. A fixed anneal time was used in these studies as representative of typical processing conditions required for bonding approaches for these films to CMOS substrates. At temperatures below 120 °C, the samples were placed directly on the metal heating element. At 120 °C and above, samples were placed on a thin glass cover slip (thickness: 100 μm) to protect the heating element. In the case of bidirectional heating, a metal tool head (8.1 × 8.3 mm^2 in area) was used to heat the top side of the sample with the bottom side heated by the hot plate, simultaneously. The force applied to the head, controlled through a lever arm, was set to 80 N. As the head size is slightly smaller than the PVDF samples, the entirety of the applied force occurs in the toolhead area; we report this as the applied pressure of 1.19 MPa.

Structural and Spectroscopic Characterization. Raman spectroscopy of the samples was carried out using a 532 nm laser (Renishaw inVia) at a power of <5 mW. To obtain the spectra, five acquisitions were averaged over nine repetitions, using a 1800 lines/mm grating. X-ray diffraction (XRD) was performed in a PANalytical XPert3 system on a rotating stage in the Bragg-Bretao geometry using a monochromatic Cu Kα source with λ = 1.5417 Å. Optical micrographs of the samples were taken in a Nikon Eclipse LV100 microscope using a 50× objective lens. Absorbance measurements were carried out using an Agilent 8453 spectrophotometer.

Piezoelectric and Pyroelectric Characterization. To measure the d_{33} piezoelectric coefficient, a commercial d_{33} piezometer system was used (Piezotest PM300). The static force was set to 10.3 N and the dynamic force was set to 0.25 N at a frequency of 110 Hz. These settings provide a system accuracy of 2%, as per the manufacturer's specifications. The electrodes of the piezometer (∼1 cm diameter) act as the metallization layer for the unmetallized PVDF. To account for any local variation within a sample, several successive measurements were taken and averaged. The PVDF samples were removed completely from the system between measurements to provide a more accurate mean and variance in the recorded d_{33}. Before the first measurement, both sides of the PVDF film under test were contacted against a grounded metal plate to remove the effects of static charge on the sample surface, and the plates of the meter were shorted as well.

To measure the voltage generated across the 1 cm^2 PVDF film during and after heating due to the pyroelectric effect, the top and bottom surfaces of the PVDF films were contacted with copper tape, allowing these surfaces to be connected to the ground and sense probes of a digital oscilloscope (Agilent Mixed-Signal Scope MSO-X 4054A) with an input capacitance of 10 pF. The 1 cm^2 piece of 200 μm PVDF has a capacitance of approximately 50 pF; this capacitance divider reduces the signal amplitude by a factor of one-sixth. We account for this by normalizing the pyroelectric voltages to the lowest measured voltage at 70 °C.

Ultrasound Testing. Ultrasound tests were performed on the same samples in a water bath with 2.5 MHz, 800 ns ultrasound pulses provided by a Verasonics P4-1 linear array probe. In these measurements, the sample was secured to a large tungsten block to ensure acoustic reflection from the substrate for maximized ultrasound signal collection. Single ultrasound pulses were transmitted, with a probe excitation voltage of 16 V_{pk-pk} in a plane-wave, resulting in an incident pressure field of approximately 260 kPa impinging on the PVDF surface, as verified with a hydrophone measurement.

RESULTS AND DISCUSSION

Long-Term Behavior of the Piezoelectric Coefficient of Heated β-PVDF. Figure 1a shows the experimental setup. With unidirectional heating above 120 °C, the films bow and become more rigid. This bowing is found to always follow the electrical polarization of the PVDF film, independent of the direction of heating: measuring the convex side with the positive electrode on the piezometer yields a positive d_{33} whereas the concave side elicits a negative d_{33}. From these observations, we associate the convex side with the positive charge and the concave side with the negative charge. The inset of Figure 1a is an optical micrograph of the sample surface showing a visible orientation of the polymer strands from the pulling process during manufacturing (the electrical poling direction itself is orthogonal to these strands). This visible macrostructure is not disturbed by heating, even at temperatures as high as 130 °C, agreeing with previous observations on the melting point of PVDF.[32] This strand orientation also indicates how the PVDF chains will bow, as indicated in the sketch in Figure 1a.

We characterized the change in the optical absorbance of 200 μm-thick PVDF films as a function of heating temperature for a single 60 s anneal using ultraviolet−visible (UV−vis) spectroscopy. Absorbance spectra in Figure 1b show a broad absorption peak in the UV region, attributed to interband electronic transitions from unoccupied π^* states in carbon.[33,34] No major changes in the absorbance occur until the material is

https://dx.doi.org/10.1021/acsapm.0c00902
ACS Appl. Polym. Mater. XXXX, XXX, XXX−XXX

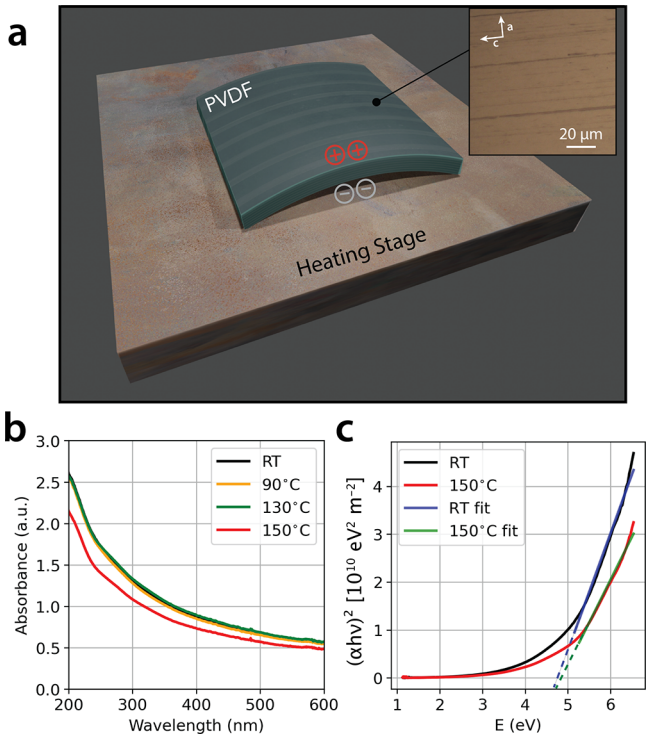

Figure 1. (a) Illustration of the experimental setup used for unidirectional heating. In the case of bidirectional heating, a metal toolhead was also used to heat the sample from the top at the same time. The bowing of the PVDF sample at high temperatures always occurs relative to the measured polarization direction. The framed inset is an optical micrograph of the sample surface, showing clearly visible directional polymer strands forming the macrostructure of the film. (b) UV−vis absorption spectra of the same 200 μm-thick β-PVDF film after heating to the labeled temperatures in a 60 s unidirectional anneal. A noticeable drop in the absorbance occurs once the sample is heated past 150 °C. (c) Tauc plot of the optical absorption response for the same sample at room temperature (RT) and after heating to 150 °C. No major shift in the optical gap is observed, suggesting that the electronic band structure of the material does not change significantly upon heating even to high temperatures.

heated to 150 °C. At this temperature, the PVDF film is observed to absorb less efficiently in the UV region, while the absorbance in the visible region remains largely unchanged. Tauc plots for the same sample at room temperature (RT) and at 150 °C are shown in Figure 1c.[35,36] An average approximate optical gap of ~4.78 ± 0.05 eV is extrapolated from linear fits to the highly absorbing regime for several samples, which is on the lower end of previous ranges observed for β-PVDF.[35,37−40] The Tauc gap here is approximate as it depends on the choice of the range for the linear fit beyond the gap energy. Upon heating to 150 °C, the absorption coefficient decreases in the film, with no significant shift in the optical gap. This suggests no major changes in the electronic band structure of the material at these temperatures, i.e., no significant amorphization. However, a change in the dielectric environment due to heat-related molecular dipole realignment is likely affecting rates of photon absorption in the material.[41]

PVDF samples of three different thicknesses were then annealed over a range of temperatures from 20 to 180 °C for 60 s. A simulation and discussion of the temperature profiles can be found in Figure S1. The d_{33} coefficients of the samples were measured once per week over the course of 4 weeks. The final piezoelectric constant for all thicknesses after 4 weeks, which we call the residual d_{33}, is plotted as a function of temperature in Figure 2a. The data are normalized to their initial values (d_{33}^0) before heating. Previous annealing studies have shown a detrimental effect on the d_{33} associated with raising the temperature above 80 °C.[30,31] However, these studies focused on isotropic heating by convection with annealing times that were 10 min or longer, leading to d_{33} losses of nearly 30% when PVDF was annealed at 100 °C. In our case, with a brief, 60 s anisotropic anneal by conduction, comparable to that in a typical pre- or postbake step in a photolithographic process, we find that PVDF can be heated to 100 °C while incurring only a 5% degradation in its d_{33}, as seen in Figure 2a. PVDF films with thickness greater than 200 μm can withstand 160 °C anneals before losing 30% of their d_{33}, although these samples suffer from significant bowing.

To examine the effect that bowing has on the residual d_{33}, we repeated the long-term unidirectional heating measurements while applying a uniform pressure, as seen in Figure S2. At or below 120 °C, no significant variation can be seen as compared to the control case with no pressure applied. Above 120 °C, bowing becomes significant enough to disturb these measurements.

The long-term stabilization plots show a negative correlation with temperature; as the annealing temperature is increased, the samples take longer to stabilize to a constant d_{33} value, as shown in Figure 2b. These long-term stabilization results also exhibit a weak thickness dependence, shown in Figure 2c. The thicker pieces of PVDF are more resilient to changes in d_{33} brought on by heating, but they also take longer to relax to their original values. An extreme case can be seen in Figure 2a: the piezoelectric response of the 28 μm piece was quenched completely after heating to 180 °C for 60 s, while the thicker 110 and 200 μm pieces retain a significant piezoelectric coefficient even at this high temperature. This is in line with theoretical calculations, showing that thicker PVDF films have a larger polarization;[42] as a result, the remnant polarization is also expected to retain a higher magnitude in thicker samples.

Crystallographic and Spectroscopic Characterization. Previous work focused on the manipulation of the dielectric properties of PVDF have emphasized the importance of surface treatment and the resulting secondary morphology,[43,44] of the relative humidity during fabrication,[45] and of the temperature[46] on the piezoelectric properties. Moreover, as PVDF is also a pyroelectric material, changes in the temperature across its polarization direction lead to a thermal destabilization of electric dipoles and an associated release of bound surface charge.[17] Here, we investigate the crystallographic changes that occur after the application of heat.

We investigated the change in the crystal structure in annealed films using XRD, as a function of both temperature and thickness. Figure 3a−c presents the raw XRD patterns obtained on 200, 110, and 28 μm films, respectively, across a series of 60 s unidirectional heating at various temperatures. The patterns are focused on the 2θ region normally associated with the (110) and (200) reflections in β-PVDF.[18,47,48] We remark that another low-intensity peak, not shown here, was also observed in our patterns around 2θ = 36.3°, which corresponds to the (020) reflection in β-PVDF,[22,49,50] and whose shift with temperature follows the same trend as the (110)/(200) peak (see Figure S3 for the full XRD spectra). As this low-angle reflection has a higher signal-to-noise ratio, we focus our discussion on it.

https://dx.doi.org/10.1021/acsapm.0c00902
ACS Appl. Polym. Mater. XXXX, XXX, XXX−XXX

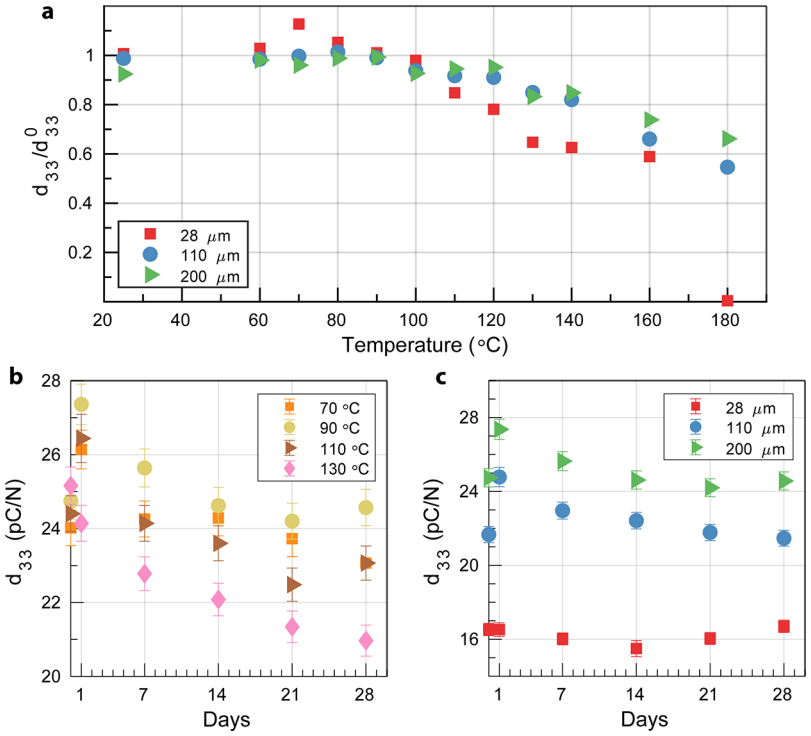

Figure 2. Long-term d_{33} responses to short 60 s anneals. Error bars show the largest possible error, either from the standard deviation of the repeated measurements or the 2% uncertainty in the meter. (a) Residual d_{33} of PVDF films of different thicknesses, measured 4 weeks after initial heating to the specified temperature. The measured standard deviations are smaller than the size of the marker. The thicker the film, the more piezoelectric functionality it retains at high temperatures. (b) d_{33} responses of 200 μm PVDF measured over 4 weeks. Transient improvements can be seen to last over 24 h for temperatures below 110 °C. (c) d_{33} responses for multiple thicknesses of PVDF annealed at 130 °C. Long-term stabilization rates can be seen to depend on thickness.

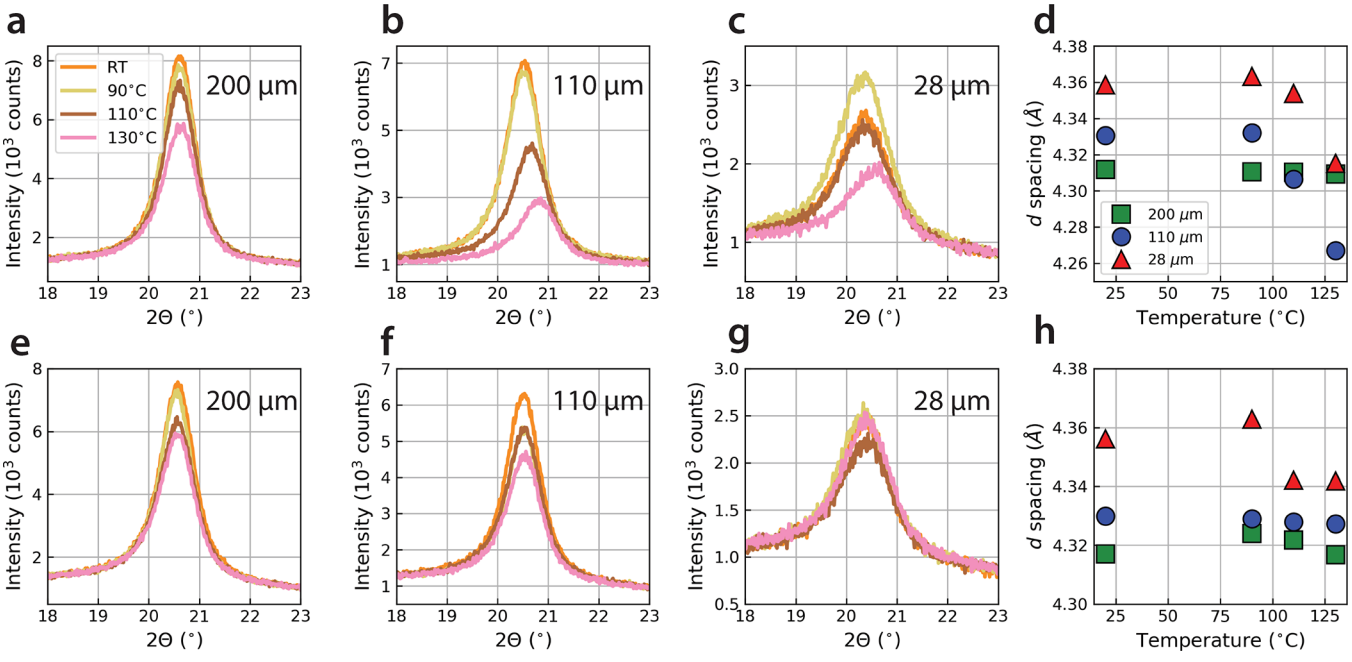

Figure 3. (a–c) XRD patterns of β-PVDF films of various thicknesses heated from one side. (d) Lattice spacings extracted from peak fits to the XRD data as a function of temperature for respective film thicknesses. A significant contraction is noted for the 110 and 28 μm films. (e–g) XRD patterns of β-PVDF films of various thicknesses heated from two sides under a pressure of 1.19 MPa. (h) Lattice spacings do not change significantly for uniformly heated samples. Note that the legend from (a) applies to (a–c) and (e–g); the legend from (d) also applies to (h).

Heating each sample unidirectionally to progressively higher temperatures affects the intensity of the diffraction peak, as well as its position. The intensity of the reflection is quenched with increasing temperature, suggesting a reduced crystallinity, or increased polymer chain disorder upon heating, i.e., smaller polymer crystallites.[20] In addition, for the thinner PVDF films,

https://dx.doi.org/10.1021/acsapm.0c00902
ACS Appl. Polym. Mater. XXXX, XXX, XXX−XXX

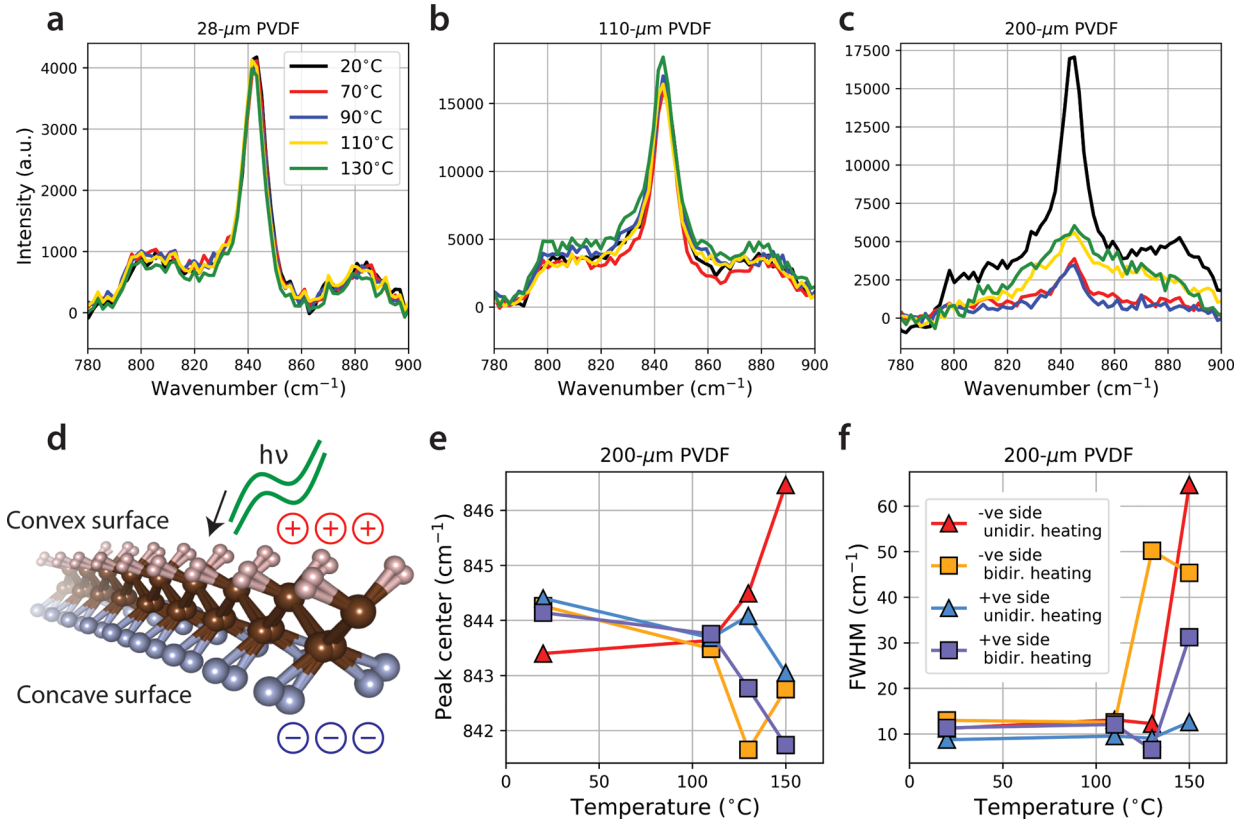

Figure 4. Raman spectroscopy of PVDF as a function of temperature and thickness. Note that the color legend in (a) applies to (a–c). (a) Raman spectra of 28 μm-thick PVDF centered at the ~840 cm^{-1} region associated with the β phase. (b) Raman spectra of 110 μm PVDF. (c) Raman spectra of 200 μm PVDF. The thickest sample shows a significant deterioration in the Raman response with increasing temperature, suggesting a change in the vibrational modes on the surface. (d) Illustration of the structure of β-PVDF strained uniaxially along the crystallographic c direction. Atoms in the figure are hydrogen (pink), carbon (brown), and fluorine (blue). The charge bubbles represent the polarization of the sample relative to the observed bowing direction for the 200 μm sample. The arrow points to the surface first sampled by incoming Raman laser light. (e) Comparison of the Raman shifts with temperature for the top and bottom surfaces of the 200 μm film when heated from one side only and from both sides at the same time. (f) Analogous data set comparing the FWHM of the fitted peaks. The same color legend applies to (e) and (f). −ve, negative; +ve, positive. The solid lines are guides to the eye in (e) and (f).

the reflection associated with the β phase shifts significantly to higher angles in the diffraction pattern due to a contraction in the lattice spacing (the d spacing) of the PVDF crystal. The untreated films have a d spacing agreeing with previously reported ranges.[51,52] (We note that the 28 μm film comes from a different manufacturer; hence, its starting d value is slightly higher.) Figure 3d tracks this contraction along the poling direction of the film (b axis), with increasing temperatures resulting in a larger reduction in the d spacing for the 110 and 28 μm samples.

To test whether the bowing of the sample during this unidirectional heating has a large influence on the lattice spacing contraction, we repeated the experiments with films which were bidirectionally heated while kept under 1.19 MPa of pressure to ensure no directional bending throughout thermal stressing. Figure 3e–g presents the XRD patterns of these samples for each respective thickness. Although the intensity of the (110)/(200) peak changes slightly with temperature for each sample, this quenching is not nearly as significant as in the case of the samples heated from one side only. Crucially, no major change in the d spacing is observed for any of the films, even for the thinnest 28 μm sample. This result suggests that the uniaxial strain suffered by samples unidirectionally heated also has a large effect on the crystal lattice of the β-PVDF and brings the polymer chains closer together along the direction of the piezoelectric polarization. This change in the dipole environment near the sample surface may lead to an increased availability of bound surface charge. It is known from scanning tunneling microscopy that surface and/or subsurface reconstruction occurs in PVDF copolymer thin films,[53,54] where the crystal structure differs from the bulk, showing more disorder in the direction perpendicular to the polymer chains. The surface dipole orientation in PVDF is also particularly sensitive to the electronic structure of the material directly interfacing the film surface, causing potential lattice constant shifts.[55] Thus, changes in the dielectric environment of the β-PVDF surface may hold the key to unlocking improved piezoelectric functionality, as has also been demonstrated recently with chemical modification[43−45] and nanoscale filler incorporation.[56]

The change in the vibrational modes of the β-PVDF films was monitored through Raman spectroscopy. The background-corrected Raman spectra presented in Figure 4a–c were fit with Voigt peaks in the region of interest, characteristic of the β phase of PVDF (840–845 cm^{-1}),[21,57] for each sample thickness, as labeled on the figure panels. This Raman mode corresponds to the antisymmetric stretching of CF_2 in β-PVDF,[58] although rocking of CH_2 is also expected to occur around this frequency regime.[18,52] Spectra of the untreated samples were best fit with multiple peaks to account for the

https://dx.doi.org/10.1021/acsapm.0c00902
ACS Appl. Polym. Mater. XXXX, XXX, XXX−XXX

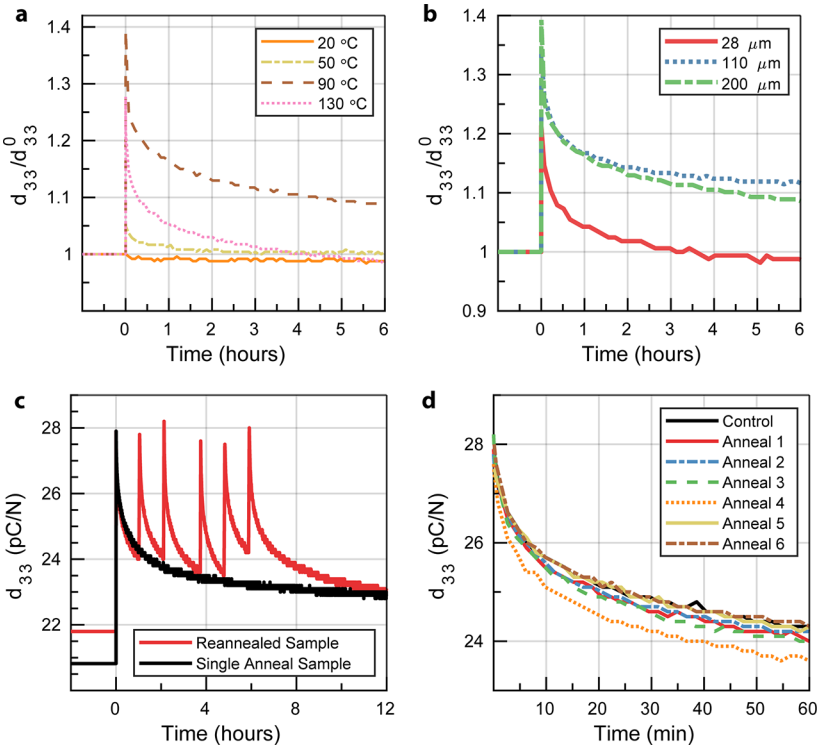

Figure 5. Short-term d_{33} responses to short 60 s anneals. (a) Normalized d_{33} responses measured over the course of several hours in 5 s intervals for 200 μm PVDF. Samples were heated at time, $t = 0$. The measurements began within 10 s after the anneal concluded. (b) Normalized d_{33} responses for 90 °C anneals for three thicknesses of PVDF. There is a weak correlation between the thickness and the spike height, while the extracted decay rates are similar across thickness. (c) d_{33} time traces of two samples of PVDF: one annealed six times, as labeled on the plot, and another annealed only once. Each anneal was 60 s at 90 °C. (d) d_{33} spikes from (a) were overlaid for easier comparison. Each spike height and decay rate is approximately the same, despite the thermal history of the sample.

shoulder peaks on either side of the most intense narrow peak. It is evident from the spectra that unidirectional heating affects the Raman modes of the PVDF films more significantly in the thicker 110 and 200 μm samples. The vibrational modes remain largely unaffected in the case of the thinnest 28 μm film, with some slight broadening and shifting occurring in the 110 μm sample. Importantly, we remark again that the thicker the sample, the larger the bowing from the center observed in the film toward the positively charged surface. The convex surface is always facing up during the Raman scan, as illustrated in Figure 4d.

Significant broadening and smearing of the peaks are observed with unidirectional heating in the 200 μm film, suggesting a change in the polarizability of the top surface on which the laser is incident during measurements. The positively charged convex side experiences a tensile strain, while the negatively charged concave side of the film experiences a compressive strain. This temperature-induced strain remains in the specimens after heating and does not relax even weeks after the initial cooling. The Raman laser probing the sample surface largely samples a strained specimen area, which may result in peak broadening and shifting.[59−61] A difference between tensile and compressive strain on the top and bottom surfaces of the film may thus present itself in Raman measurements in the form of peak shifts in opposite directions. Computational work has previously shown that changing the surface termination of the PVDF unit cell affects the position of the vibrational modes,[62] which may be the case if terminal hydrogens/flourines are brought closer together/further apart when the polymer chain is under strain.

To create this condition, we heated a 200 μm sample unidirectionally, but this time, we took the Raman spectra on both the top and bottom surfaces of the sample. We compared the observed Raman shifts with temperature with another 200 μm sample that was heated bidirectionally and held under 1.19 MPa of pressure in the same manner as the XRD studies such that bowing did not occur (see Figure S4 for the raw bidirectional Raman spectra). Figure 4e tracks these shifts from fitted peaks explicitly on the same plot. In the case of the sample heated from both sides, which did not bend, the peak centers are seen to downshift slightly with temperature relative to the untreated sample, for both surfaces. In contrast, the sample that is heated unidirectionally and visibly bows shows divergent peak shifts. The convex, positively charged surface upshifts several wavenumbers with temperature, while the concave, negatively charged surface downshifts with temperature relative to the untreated film. Figure 4f shows the full width at half-maxima (FWHM) of fits from the same data set, showing that above 130 °C, the vibrational modes of the sample surface (for both unidirectional and bidirectional heating) lose integrity as the crystal becomes more and more strained away from its natural structure. For examples of Raman fits to the raw spectra for both cases, see Figure S5.

Despite no major change in the bulk crystal structure of the film, as observed from XRD, our Raman results indicate tensile top surface and compressive bottom surface strain in the heavily bowed 200 μm film. Importantly, the surface strain observations correlate with residual d_{33} values being higher for the thicker samples, i.e., surface strain leads to a higher residual d_{33}. Moreover, no significant change in the ratio of the α-phase

https://dx.doi.org/10.1021/acsapm.0c00902
ACS Appl. Polym. Mater. XXXX, XXX, XXX−XXX

to β-phase of PVDF content was seen after heat treatments from the Raman spectra,[57] confirming that no mesoscopic change in the crystal structure of the polymer film occurs during the heating. This result agrees with prior evidence that random thermal depolarization due to surface charge release is the source of changes in the d_{33}, rather than large-scale changes in the crystal structure of the polymer.[31] This is also consistent with results from other works in which it has been demonstrated that increasing surface strain in PVDF films by forming kirigami cuts boosts the generated piezoelectric charge multifold for a similar starting d_{33} value.[63] This observation suggests that manipulation of surface strain has considerable effects on the piezoelectric response of the material.

To assert that this strain asymmetry is responsible for the remnant piezoelectric behavior, we compared the residual d_{33} of samples heated bidirectionally to samples heated unidirectionally at a selection of temperatures. These data are presented in Figure S6, where unidirectionally heated samples have higher residual d_{33} values than bidirectionally heated samples. Furthermore, we explored the effects of longer anneals, showing a greater divergence between the residual piezoelectric effect between bidirectional and unidirectional heating, as shown in Figure S7.

Short-Term Behavior of the Piezoelectric Coefficient of Heated β-PVDF. Interestingly, we also observed that the d_{33} decay is interrupted by a transient increase in the early stages of cooling, spiking well above its pre-heated value. This increase can last up to 72 h after a unidirectional annealing procedure and is reproducible across a wide array of temperatures; the first 6 h are shown in Figure 5a,b. The normalized increase in the d_{33}, or the measured spike height, exhibits a strong dependence on temperature and a weak dependence on thickness. The observed decays associated with its relaxation over the next days and weeks also vary strongly with annealing temperature and weakly with thickness.

This transient improvement in the d_{33} immediately after heating can be repeated on samples regardless of their annealing history. If a sample has already been annealed, heating the sample again causes another spike in the d_{33}, as shown in Figure 5c for a representative 110 μm sample. There is a negligible long-term difference in the d_{33} value when compared to a reference piece of 110 μm-thick PVDF, which was heated only once. Figure 5d overlays the spike transients to show that the decay rates in a reannealed sample are similar after each annealing event and similar to the decay of a piece annealed only once. This repeatability indicates that the transient d_{33} spike is not due to a permanent change in the structure of the semicrystalline polymer and that its source can be reliably reactivated by increasing the temperature again.

Since PVDF is also a pyroelectric material, temporal thermal gradients can cause a potential difference to develop across the sample.[64] To examine any correlation between the pyroelectricity of the material and the observed d_{33} enhancement, the resulting pyroelectric voltage was measured as a function of temperature, T. The heating profiles used to anneal the PVDF can be seen in Figure 6a. The sharp drops in temperature to 20 °C correspond to lifting the PVDF piece off the heating stage. The pyroelectric response depends on both ΔT and $|\partial^2 T/\partial t^2|$ and manifests as significant voltage shifts at the sharp corners of the heating profile. If the pyroelectric effect was responsible for releasing the free charge that boosts the d_{33}, then one may expect that varying ΔT and $|\partial^2 T/\partial t^2|$ would yield a correlation between the d_{33} spike height and the generated pyroelectric

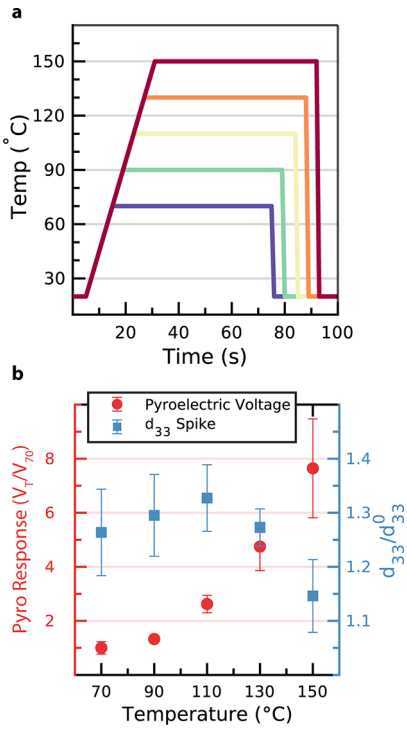

Figure 6. (a) Heating profiles used to examine the pyroelectric effect. Initial heating ramp rates were kept constant to avoid additional changes in $|\partial^2 T/\partial t^2|$ outside of the end drop. (b) Comparison of pyroelectric and piezoelectric responses. The pyroelectric response is normalized to the response measured at 70 °C. Error bars on each trace represent the standard deviation of the measurements.

voltage. We tested this theory by heating the 200 μm PVDF film to different temperatures, thereby varying ΔT, and observed a close-to-linear scaling in the generated voltage, consistent with the pyroelectric effect. The generated potential differences across the PVDF film are plotted along with the normalized magnitudes of the d_{33} spike in Figure 6b. The traces have no correlation, diverging strongly at higher temperatures, indicating that free charge generated by the pyroelectric effect is decoupled from the effect of boosting the piezoelectric charge generation.

The decay rate of the d_{33} spike may provide insight into the origin of this phenomenon. The empirical thickness-normalized decay rate is best fitted with a power law of the form:

$$d_{33}(t) \propto t^{-B} \tag{1}$$

where B is always between 0 and 1 in our measured samples. While such a decaying power law model is also characteristic of current discharge in dielectrics, described commonly by the empirical Curie−von Schweidler relation and has previously been used to characterize PVDF copolymers and other polymer blends,[65−67] we found little evidence that the excess free charge boosting the d_{33} arises from this effect. This effect is usually reported as a response to sharp changes in the displacement field across a dielectric. A dielectric discharge model, however, is inconsistent with the observations here. The time frame of these decays is usually on the scale of tens of minutes,[67] while our results in Figure 2a,b show stabilization only after many hours or days. Furthermore, the poling fields used to study this effect are typically in the tens of kV cm^{-1}, whereas the generated fields we measure in Figure 6b are on

https://dx.doi.org/10.1021/acsapm.0c00902
ACS Appl. Polym. Mater. XXXX, XXX, XXX−XXX

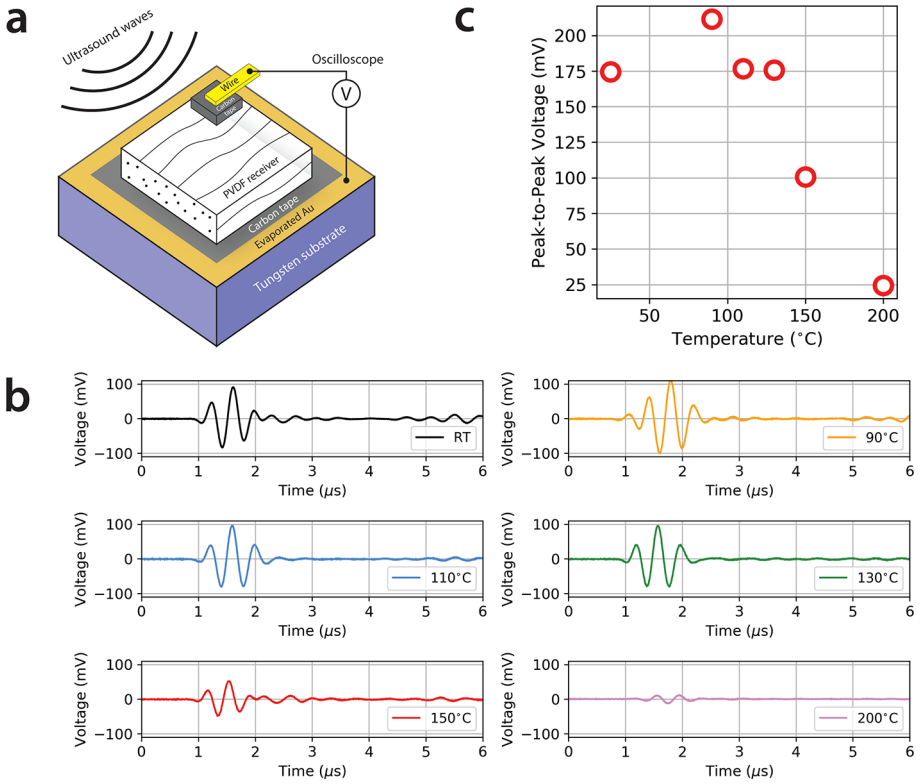

Figure 7. (a) Sketch of the experimental ultrasound receiver setup. The PVDF transducer is adhered to a metallized glass substrate with carbon tape on the bottom. On its top surface, carbon tape is also used to contact a wire to the corner of the receiver. Wavy lines in the illustration symbolize the visible direction of the polymer strands. (b) Ultrasound-induced alternating voltage traces measured across the PVDF receiver as a function of heating temperature for the same 200 μm PVDF piece. (c) Peak-to-peak voltage amplitude transduced by the receiver as a function of temperature. The trend in the data follows the trend in the d_{33} response from Figure 2a.

the order of 0.01 kV cm^{-1}. It is thus unlikely that the voltages generated by heating in our samples affect the current discharge.

We instead propose that the origin of the spikes arises from a mechanical response to strain. In our crystallographic and spectroscopic examination of PVDF, we observed that unidirectional heating causes stress on the crystal structure and the film surface. Of relevance here is the work of Katsouras et al., where the crystal lattice dynamics due to the piezoelectric effect were monitored with *in situ* XRD.[68] Changes in the lattice constant of the semiamorphous P(VDF-TrFE) copolymer were found to be coupled to volume changes in the amorphous regions, which led to an increase in the interfacial capacitance between crystalline and amorphous domains, on average resulting in a higher charge density generated on the film surface. These results are likely to also translate to β-PVDF.[69] It is possible that the orientation of the dipole domains, responsible for the piezoelectric effect, may mechanically shift during heating, providing surplus charge to the film surface through this constrictive capacitance increase. This may temporarily increase the d_{33} of the material. The decay rate, with characteristic decay times measured in days, may then be related to the gradual recapturing and trapping of these free charges back into the polymer domains through mechanical relaxation. Mechanical relaxation has been previously observed after stretching PVDF to create high β phase-content samples.[70] This reorientation and associated charge recapture may be subject to percolation-like effects in this network of crystalline lamellae embedded in amorphous domains, bringing about the observed power law dependence, which qualitatively mirrors dielectric discharge. Further studies using advanced *in situ* spectroscopic and crystallographic methods are needed to unveil the exact microscopic mechanism, while modeling of network criticality may clarify the nature of the charge increase around the percolation threshold in such an interconnected capacitive network. To confirm our assertion that the spiking behavior correlates with strain, we examined the spike magnitude for both unidirectionally and bidirectionally heated samples (see Figure S8). We observed a diminished response in the case of bidirectional heating at high temperatures relative to unidirectional heating, suggesting that the strain asymmetry observed in characterization has a substantial effect on the piezoelectric performance.

Ultrasound Receiver Testing. In addition to the direct measurements of the d_{33} spike, we found that the thermally induced improved piezoelectric response enhanced the sensitivity of an ultrasonic transducer fabricated from this material. PVDF is an exceptional ultrasound receiver in that it has a high piezoelectric receiving constant of $g_{33} = d_{33}/(\varepsilon_0\varepsilon_r) \approx$ 220 mV m N^{-1}, where ε_0 is the permittivity of free space and $\varepsilon_r \approx 12$.

As initially shown in Figure 2c,d, one expects a spike in the d_{33}, and thus the piezoelectric response, minutes within the thermal annealing event. All ultrasound tests were conducted within 5 min of heating. The testing setup is demonstrated in Figure 7a, where conductive carbon tape was used to electrically connect to either side of the PVDF. Although the oscilloscope used to measure this signal is set to have an input impedance of 1 MΩ, some voltage division is still present due

https://dx.doi.org/10.1021/acsapm.0c00902
ACS Appl. Polym. Mater. XXXX, XXX, XXX−XXX

to the capacitive division between the probe and the PVDF. As these losses are the same for each test, they are neglected in this analysis. The same piece of PVDF was reused for each temperature to have the same baseline, increasing monotonically in temperature for each step. Reusing the PVDF is unlikely to introduce any error as Figure 5a shows the same trend even with several reanneals.

The resulting voltage traces from the ultrasound excitations for each temperature are shown in Figure 7b. Exactly one bipolar pulse was sent for each test; however, some initial ringing is seen after the peak due to the mismatch between the acoustic impedance of PVDF and the tungsten block. Following the observed d_{33} trend for 200 μm PVDF, Figure 7c shows how the peak-to-peak piezoelectric voltage across the transducer induced by ultrasound waves experiences a maximum at 90 °C, before sharply reducing in amplitude above 130 °C. The response at 200 °C is nearly completely quenched as the material goes through its glass transition above 180 °C.

CONCLUSIONS

In conclusion, the long- and short-term piezoelectric responses of PVDF to thermal treatment mimicking typical microfabrication conditions were investigated. Our experiments show that short exposure to common temperatures experienced in photolithographic processes (up to 100 °C) have no long-term negative effects on the piezoelectric coefficient of PVDF when unidirectionally applied. These results contradict previously held notions restricting processing temperatures to less than 80 °C. Moreover, this increases the potential thermal budget for bonding steps and other processing. When examining the crystal structure changes, we found evidence that strained samples have a higher residual d_{33}. In addition to the expected long-term degradation of the d_{33} due to the depoling of the dipole moments in the polymer, we observed a repeatable, transient increase in the piezoelectric constant of the material. Our results are of interest to the ultrasound transducer community and groups working on micromachining and the direct integration of prepoled piezoelectric PVDF on CMOS substrates.

ASSOCIATED CONTENT

Supporting Information

The Supporting Information is available free of charge at https://pubs.acs.org/doi/10.1021/acsapm.0c00902.

COMSOL heat propagation, d_{33} versus temperature for various pressure, full-range XRD spectra, raw Raman spectra after bidirectional heating, fits to the Raman spectra, d_{33} versus temperature response comparison between unidirectional and bidirectional heating, d_{33} versus annealing time response comparison between unidirectional and bidirectional heating, and transient d_{33} spike comparison between unidirectional and bidirectional heating (PDF)

AUTHOR INFORMATION

Corresponding Author

Jeffrey D. Sherman − *Department of Electrical Engineering, Columbia University, New York, New York 10027, United States;* orcid.org/0000-0001-5182-9036; Email: jds2245@columbia.edu

Authors

Jeffrey Elloian − *Department of Electrical Engineering, Columbia University, New York, New York 10027, United States;* orcid.org/0000-0003-0873-3164

Jakub Jadwiszczak − *Department of Electrical Engineering, Columbia University, New York, New York 10027, United States;* orcid.org/0000-0002-9518-9402

Kenneth L. Shepard − *Department of Electrical Engineering and Department of Biomedical Engineering, Columbia University, New York, New York 10027, United States;* orcid.org/0000-0003-0665-6775

Complete contact information is available at: https://pubs.acs.org/10.1021/acsapm.0c00902

Author Contributions

§J.D.S and J.E. contributed equally.

Notes

The authors declare no competing financial interest.

ACKNOWLEDGMENTS

The authors thank John Barth for assistance with the Fineplacer and Megan Noga for collecting some of the long-term d_{33} data. This work was supported by the National Institute of Health under Grant U01NS099717.

REFERENCES

(1) Wygant, I. O.; Zhuang, X.; Yeh, D. T.; Oralkan, O.; Ergun, A. S.; Karaman, M.; Khuri-Yakub, B. T. Integration of 2D CMUT Arrays with Front-End Electronics for Volumetric Ultrasound Imaging. *IEEE Trans. Ultrason. Ferroelectr. Freq. Control* **2008**, *55*, 327−342.

(2) Seok, C.; Wu, X.; Yamaner, F. Y.; Oralkan, Ö. A front-end integrated circuit for a 2D capacitive micromachined ultrasound transducer (CMUT) array as a noninvasive neural stimulator. *2017 IEEE International Ultrasonics Symposium (IUS)*; IEEE: 2017, 1−4.

(3) Shi, C.; Costa, T.; Elloian, J.; Shepard, K. L. Monolithic Integration of Micron-Scale Piezo-electric Materials with CMOS for Biomedical Applications. *International Electron Devices Meeting. IEDM Technical Digest*; IEEE: 2018, 2018-*Decem*, 4−5.

(4) Basiri-Esfahani, S.; Armin, A.; Forstner, S.; Bowen, W. P. Precision Ultrasound Sensing on a Chip. *Nat. Commun.* **2019**, *10*, 132.

(5) Sinha, T. K.; Ghosh, S. K.; Maiti, R.; Jana, S.; Adhikari, B.; Mandal, D.; Ray, S. K. Graphene-Silver-Induced Self-Polarized PVDF-Based Flexible Plasmonic Nanogenerator toward the Realization for New Class of Self Powered Optical Sensor. *ACS Appl. Mater. Interfaces* **2016**, *8*, 14986−14993.

(6) Gao, S.; Wu, X.; Ma, H.; Robertson, J.; Nathan, A. Ultrathin Multifunctional Graphene-PVDF Layers for Multidimensional Touch Interactivity for Flexible Displays. *ACS Appl. Mater. Interfaces* **2017**, *9*, 18410−18416.

(7) Elfrink, R.; Kamel, T. M.; Goedbloed, M.; Matova, S.; Hohlfeld, D.; van Andel, Y.; van Schaijk, R. Vibration Energy Harvesting with Aluminum Nitride-based Piezoelectric Devices. *J. Micromech. Microeng.* **2009**, *19*, No. 094005.

(8) Garain, S.; Sinha, T. K.; Adhikary, P.; Henkel, K.; Sen, S.; Ram, S.; Sinha, C.; Schmeißer, D.; Mandal, D. Self-Poled Transparent and Flexible UV Light-emitting Cerium Complex−PVDF Composite: A High-Performance Nanogenerator. *ACS Appl. Mater. Interfaces* **2015**, *7*, 1298−1307.

(9) Sultana, A.; Sadhukhan, P.; Alam, M. M.; Das, S.; Middya, T. R.; Mandal, D. Organo-Lead Halide Perovskite Induced Electroactive β-Phase in Porous PVDF Films: An Excellent Material for Photoactive Piezoelectric Energy Harvester and Photodetector. *ACS Appl. Mater. Interfaces* **2018**, *10*, 4121−4130.

(10) Xie, Y.; Jiang, W.; Fu, T.; Liu, J.; Zhang, Z.; Wang, S. Achieving High Energy Density and Low Loss in PVDF/BST Nanodielectrics

with Enhanced Structural Homogeneity. *ACS Appl. Mater. Interfaces* **2018**, *10*, 29038−29047.
(11) Foster, F. S.; Harasiewicz, K. A.; Sherar, M. D. A History of Medical Biological Imaging with Polyvinylidene Fluoride (PVDF) Transducers. *IEEE Trans. Ultrason. Ferroelectr. Freq. Control* **2000**, *47*, 1363−1371.
(12) Caliano, G.; Matrone, G.; Savoia, A. S. Biasing of Capacitive Micromachined Ultrasonic Transducers. *IEEE Trans. Ultrason. Ferroelectr. Freq. Control* **2017**, *64*, 402−413.
(13) Chen, C.; Raghunathan, S. B.; Yu, Z.; Shabanimotlagh, M.; Chen, Z.; Chang, Z.-y.; Blaak, S.; Prins, C.; Ponte, J.; Noothout, E.; Vos, H. J.; Bosch, J. G.; Verweij, M. D.; de Jong, N.; Pertijs, M. A. P. A Prototype PZT Matrix Transducer with Low-Power Integrated Receive ASIC for 3-D Transesophageal Echocardiography. *IEEE Trans. Ultrason. Ferroelectr. Freq. Control* **2016**, *63*, 47−59.
(14) Costa, T.; Shi, C.; Tien, K.; Shepard, K. L. A CMOS 2D Transmit Beamformer with Integrated PZT Ultrasound Transducers for Neuromodulation. *2019 IEEE Custom Integrated Circuits Conference (CICC)*; 2019; pp. 1−4.
(15) Murayama, N.; Nakamura, K.; Obara, H.; Segawa, M. The Strong Piezoelectricity in Polyvinylidene Fluroide (PVDF). *Ultrasonics* **1976**, *14*, 15−24.
(16) Hasegawa, R.; Takahashi, Y.; Chatani, Y.; Tadokoro, H. Crystal Structures of Three Crystalline Forms of Poly(vinylidene fluoride). *Polym. J.* **1972**, *3*, 600−610.
(17) Wan, C.; Bowen, C. R. Multiscale-structuring of Polyvinylidene Fluoride for Energy Harvesting: the Impact of Molecular-, Micro- and Macro-Structure. *J. Mater. Chem. A* **2017**, *5*, 3091−3128.
(18) Martins, P.; Lopes, A. C.; Lanceros-Mendez, S. Electroactive Phases of Poly(vinylidene fluoride): Determination, Processing and Applications. *Prog. Polym. Sci.* **2014**, *39*, 683−706.
(19) Wang, J.; Li, H.; Liu, J.; Duan, Y.; Jiang, S.; Yan, S. On the $\alpha \rightarrow \beta$ Transition of CarbonCoated Highly Oriented PVDF Ultrathin Film Induced by Melt Recrystallization. *J. Am. Chem. Soc.* **2003**, *125*, 1496−1497.
(20) Yee, W. A.; Kotaki, M.; Liu, Y.; Lu, X. Morphology, Polymorphism Behavior and Molecular Orientation of Electrospun Poly(vinylidene fluoride) Fibers. *Polymer* **2007**, *48*, 512−521.
(21) Constantino, C. J. L.; Job, A. E.; Simões, R. D.; Giacometti, J. A.; Zucolotto, V.; Oliveira, O. N., Jr.; Gozzi, G.; Chinaglia, D. L. Phase Transition in Poly(vinylidene fluoride) Investigated with Micro-Raman Spectroscopy. *Appl. Spectrosc.* **2005**, *59*, 275−279.
(22) Hattori, T.; Kanaoka, M.; Ohigashi, H. Improved Piezoelectricity in Thick Lamellar β-Form Crystals of Poly(vinylidene fluoride) Crystallized under High Pressure. *J. Appl. Phys.* **1996**, *79*, 2016−2022.
(23) Jain, A.; Kumar, J.; Mahapatra, D. R.; Kumar, H. H. Detailed studies on the formation of piezo-electric β-phase of PVDF at different hot-stretching conditions. *Sensors and Smart Structures Technologies for Civil, Mechanical, and Aerospace Systems*; International Society for Optics and Photonics: 2010. *7647*; pp. 733−743.
(24) Matsushige, K.; Nagata, K.; Imada, S.; Takemura, T. The II-I Crystal Transformation of Poly(vinylidene fluoride) under Tensile and Compressional Stresses. *Polymer* **1980**, *21*, 1391−1397.
(25) Yu, Y.-J.; McGaughey, A. J. H. Energy Barriers for Dipole Moment Flipping in PVDF-Related Ferroelectric Polymers. *J. Chem. Phys.* **2016**, *144*, No. 014901.
(26) Zou, W.; Holland, S.; Kim, K. Y.; Sachse, W. Wideband High-Frequency Line-Focus PVDF Transducer for Materials Characterization. *Ultrasonics* **2003**, *41*, 157−161.
(27) Kimura, K.; Ohigashi, H. Generation of Very High-Frequency Ultrasonic Waves Using Thin Films of Vinylidene Fluoride-Trifluoroethylene Copolymer. *J. Appl. Phys* **1987**, *61*, 4749−4754.
(28) Kim, H.-J.; Ziaie, B. Fabrication Techniques for Improving the Performance of PVDF-on-Silicon Ultrasonic Transducer Arrays. *2006 International Conference of the IEEE Engineering in Medicine and Biology Society*; IEEE: 2006; 3491−3494.
(29) Bezaitis, K.; Papathanassiou, A. N.; Sakellis, E. Piezoelectric Polyvinylidene Fluoride-Based Epoxy Composites Produced by Combined Uniaxial Compression and Poling. *Appl. Phys. Lett.* **2019**, *115*, 192902.
(30) Eberle, G.; Eisenmenger, W. Thermal depolarization of PVDF: anomaly at 180 degrees C. *IEEE Trans. Electr. Insul.* **1991**, 768−772.
(31) Dargaville, T. R.; Celina, M.; Chaplya, P. M. Evaluation of Piezoelectric Poly(vinylidene fluoride) Polymers for Use in Space Environments. I. Temperature Limitations. *J. Polym. Sci., Part B: Polym. Phys.* **2005**, *43*, 1310−1320.
(32) Lovinger, A. J.; Davis, D. D.; Cais, R. E.; Kometani, J. M. On the Curie Temperature of Poly(vinylidene fluoride). *Macromolecules* **1986**, *19*, 1491−1494.
(33) Takagi, Y.; Okada, S. Theoretical Calculation for the Ultraviolet Optical Properties of Single-Walled Carbon Nanotubes. *Phys. Rev. B* **2009**, *79*, 233406.
(34) Pang, S.; Hernandez, Y.; Feng, X.; Müllen, K. Graphene as Transparent Electrode Material for Organic Electronics. *Adv. Mater.* **2011**, *23*, 2779−2795.
(35) Batra, A.; Kassu, A.; Curley, M.; Sampson, J.; Palwai, S.; Showe, A. Optical Parametric Investigation on a Poled PVDF Thin-Film for Optoelectronic Devices. *Sens. Transducers* **2019**, *236*, 1−6.
(36) Indolia, A. P.; Gaur, M. S. Optical Properties of Solution Grown PVDF-ZnO Nanocomposite Thin Films. *J. Polym. Res.* **2012**, *20*, 43.
(37) Elashmawi, I. S.; Hakeem, N. A. Effect of PMMA Addition on Characterization and Morphology of PVDF. *Polym. Eng. Sci.* **2008**, *48*, 895−901.
(38) Jana, S.; Garain, S.; Sen, S.; Mandal, D. The Influence of Hydrogen Bonding on the Dielectric Constant and the Piezoelectric Energy Harvesting Performance of Hydrated Metal Salt Mediated PVDF Films. *Phys. Chem. Chem. Phys.* **2015**, *17*, 17429−17436.
(39) Devi, P. I.; Ramachandran, K. Dielectric Studies on Hybridised PVDF-ZnO Nanocomposites. *J. Exp. Nanosci.* **2011**, *6*, 281−293.
(40) Mandal, D.; Henkel, K.; Müller, K.; Schmeißer, D. Bandgap Determination of P(VDF-TrFE) Copolymer Film by Electron Energy Loss Spectroscopy. *Bull. Mater. Sci.* **2010**, *33*, 457−461.
(41) Backlund, M. P.; Lew, M. D.; Backer, A. S.; Sahl, S. J.; Moerner, W. E. The Role of Molecular Dipole Orientation in Single-Molecule Fluorescence Microscopy and Implications for SuperResolution Imaging. *ChemPhysChem* **2014**, *15*, 587−599.
(42) Nakhmanson, S. M.; Nardelli, M. B.; Bernholc, J. Collective polarization effects in β-polyvinylidene fluoride and its copolymers with tri- and tetrafluoroethylene. *Phys. Rev. B* **2005**, *72*, 115210.
(43) Zaarour, B.; Zhu, L.; Huang, C.; Jin, X. Controlling the Secondary Surface Morphology of Electrospun PVDF Nanofibers by Regulating the Solvent and Relative Humidity. *Nanoscale Res. Lett.* **2018**, *13*, 1−11.
(44) Zhang, Y.; Ye, L.; Zhang, B.; Chen, Y.; Zhao, W.; Yang, G.; Wang, J.; Zhang, H. Characteristics and Performance of PVDF Membrane Prepared by Using NaCl Coagulation Bath: Relationship Between Membrane Polymorphous Structure and Organic Fouling. *J. Membr. Sci.* **2019**, *579*, 22−32.
(45) Szewczyk, P. K.; Gradys, A.; Kim, S. K.; Persano, L.; Marzec, M.; Kryshtal, A.; Busolo, T.; Toncelli, A.; Pisignano, D.; Bernasik, A.; Kar-Narayan, S.; Sajkiewicz, P.; Stachewicz, U. Enhanced Piezoelectricity of Electrospun Polyvinylidene Fluoride (PVDF) Fibers for Energy Harvesting. *ACS Appl. Mater. Interfaces* **2020**, *12*, 13575−13583.
(46) Gregorio, R., Jr.; Ueno, E. M. Effect of Crystalline Phase, Orientation and Temperature on the Dielectric Properties of Poly (vinylidene fluoride) (PVDF). *J. Mater. Sci.* **1999**, *34*, 4489−4500.
(47) Li, X.; Zhou, C.; Du, R.; Li, N.; Han, X.; Zhang, Y.; An, S.; Xiao, C. Evolution of Polyvinylidene Fluoride (PVDF) Hierarchical Morphology during Slow Gelation Process and Its Superhydrophobicity. *ACS Appl. Mater. Interfaces* **2013**, *5*, 5430−5435.
(48) Li, L.; Zhang, M.; Rong, M.; Ruan, W. Studies on the Transformation Process of PVDF from α to β Phase by Stretching. *RSC Adv.* **2014**, *4*, 3938−3943.

https://dx.doi.org/10.1021/acsapm.0c00902
ACS Appl. Polym. Mater. XXXX, XXX, XXX−XXX

(49) Mohammadi, B.; Yousefi, A. A.; Bellah, S. M. Effect of Tensile Strain Rate and Elongation on Crystalline Structure and Piezoelectric Properties of PVDF Thin Films. *Polym. Test.* **2007**, *26*, 42−50.
(50) Esterly, D. M.; Love, B. J. Phase Transformation to β-Poly(vinylidene fluoride) by Milling. *J. Polym. Sci., Part B: Polym. Phys.* **2003**, *42*, 91−97.
(51) Jurczuk, K.; Galeski, A.; Mackey, M.; Hiltner, A.; Baer, E. Orientation of PVDF α and γ Crystals in Nanolayered Films. *Colloid Polym. Sci.* **2015**, *293*, 1289−1297.
(52) Gregorio, R., Jr. Determination of the α, β, and γ Crystalline Phases of Poly(vinylidene fluoride) Films Prepared at Different Conditions. *J. Appl. Polym. Sci.* **2006**, *100*, 3272−3279.
(53) Li, J. C.; Zhang, R. Q.; Wang, C. L.; Wong, N. B. Effect of thickness on the electronic structure of poly(vinylidene fluoride) molecular films from first-principles calculations. *Phys. Rev. B* **2007**, *75*, 155408.
(54) Choi, J.; Dowben, P. A.; Ducharme, S.; Fridkin, V. M.; Palto, S. P.; Petukhova, N.; Yudin, S. G. Lattice and Electronic Band Structure Changes across the Surface Ferroelectric Transition. *Phys. Lett. A* **1998**, *249*, 505−511.
(55) Duan, C.-g.; Mei, W. N.; Yin, W.-G.; Liu, J.; Hardy, J. R.; Ducharme, S.; Dowben, P. A. Simulations of ferroelectric polymer film polarization: The role of dipole interactions. *Phys. Rev. B* **2004**, *69*, 235106.
(56) Barrau, S.; Ferri, A.; Da Costa, A.; Defebvin, J.; Leroy, S.; Desfeux, R.; Lefebvre, J.-M. Nanoscale Investigations of α- and γ-Crystal Phases in PVDF-Based Nanocomposites. *ACS Appl. Mater. Interfaces* **2018**, *10*, 13092−13099.
(57) Riosbaas, M. T.; Loh, K. J.; O'Bryan, G.; Loyola, B. R. *In situ* Phase Change Characterization of PVDF Thin Films Using Raman Spectroscopy. *Sensors and Smart Structures Technologies for Civil, Mechanical, and Aerospace Systems 2014*; International Society for Optics and Photonics: 2014; p 90610Z.
(58) Ruan, L.; Yao, X.; Chang, Y.; Zhou, L.; Qin, G.; Zhang, X. Properties and Applications of the β Phase Poly(vinylidene fluoride). *Polymer* **2018**, *10*, 228.
(59) Gayle, A. J.; Friedman, L. H.; Beams, R.; Bush, B. G.; Gerbig, Y. B.; Michaels, C. A.; Vaudin, M. D.; Cook, R. F. Two-Dimensional Strain-mapping by Electron Backscatter Diffraction and Confocal Raman Spectroscopy. *J. Appl. Phys.* **2017**, *122*, 205101.
(60) Mohiuddin, T. M. G.; Lombardo, A.; Nair, R. R.; Bonetti, A.; Savini, G.; Jalil, R.; Bonini, N.; Basko, D. M.; Galiotis, C.; Marzari, N.; Novoselov, K. S.; Geim, A. K.; Ferrari, A. C. Uniaxial strain in graphene by Raman spectroscopy: *G* peak splitting, Grüneisen parameters, and sample orientation. *Phys. Rev. B* **2009**, *79*, 205433.
(61) Chandrasekhar, M.; Renucci, J. B.; Cardona, M. Effects of interband excitations on Raman phonons in heavily doped *n*−Si. *Phys. Rev. B* **1978**, *17*, 1623−1633.
(62) Nakhmanson, S. M.; Korlacki, R.; Johnston, J. T.; Ducharme, S.; Ge, Z.; Takacs, J. M. Vibrational properties of ferroelectric β-vinylidene fluoride polymers and oligomers. *Phys. Rev. B* **2010**, *81*, 174120.
(63) Hu, N.; Chen, D.; Wang, D.; Huang, S.; Trase, I.; Grover, H. M.; Yu, X.; Zhang, J. X. J.; Chen, Z. Stretchable Kirigami Polyvinylidene Difluoride Thin Films for Energy Harvesting: Design, Analysis, and Performance. *Phys. Rev. Appl.* **2018**, *9*, No. 021002.
(64) Wada, Y.; Hayakawa, R. Piezoelectricity and Pyroelectricity of Polymers. *Jpn. J. Appl. Phys.* **1976**, *15*, 2041−2057.
(65) Molinié, P. Charge Injection in Corona-Charged Polymeric Films: Potential Decay and Current Measurements. *J. Electrost.* **1999**, *45*, 265−273.
(66) Saxena, P.; Gaur, M. S. Transient Current Characteristics in PVDF-PSF Blend Samples. *J. Integr. Sci. Technol.* **2018**, *6*, 37−45.
(67) Saxena, P.; Shukla, P.; Gaur, M. S. An Investigation on Transient Current Characteristics in Polymeric Double Layer Thin Films. *J. Integr. Sci. Technol.* **2019**, *7*, 1−9.
(68) Katsouras, I.; Asadi, K.; Li, M.; van Driel, T. B.; Kjær, K. S.; Zhao, D.; Lenz, T.; Gu, Y.; Blom, P. W. M.; Damjanovic, D.; Nielsen, M. M.; de Leeuw, D. M. The Negative Piezoelectric Effect of the Ferroelectric Polymer Poly(vinylidene fluoride). *Nat. Mater.* **2015**, *15*, 78−84.
(69) Furukawa, T.; Seo, N. Electrostriction as the Origin of Piezoelectricity in Ferroelectric Polymers. *Jpn. J. Appl. Phys.* **1990**, *29*, 675−680.
(70) Grubb, D. T.; Kearney, F. R. Zone Drawing and Mechanical Relaxation of Poly(vinylidene fluoride). *J. Polym. Sci., Part B: Polym. Phys.* **1990**, *28*, 2071−2078.

https://dx.doi.org/10.1021/acsapm.0c00902
ACS Appl. Polym. Mater. XXXX, XXX, XXX−XXX